

Active pitch control of tethered wings for airborne wind energy

M. Buffoni, B. Galletti, J. Ferreau, L. Fagiano, and M. Mercangoez

Abstract—A study on the aerodynamics and on the active pitch control of curved tethered wings for airborne wind energy is presented. Computational fluid dynamics techniques, previously validated with experimental data, are used to derive the aerodynamic coefficients of a curved kite as a function of the angle of attack. In contrast with previous results, such analysis indicates that the kite efficiency is quite flat over a wide range of values of the angle of attack. Based on such analysis, an active pitch control strategy is proposed, which is able to maximize the generated traction force during operation without requiring neither an estimate of the angle of attack, nor an accurate model of the system's dynamics.

I. INTRODUCTION

The last decade has seen a steadily increasing number of researchers and small companies developing a new class of renewable energy generators, falling under the umbrella name of airborne wind energy (AWE), which employ autonomous tethered wings or kites to convert wind energy into mechanical and then electrical power (see e.g. [1], [2]). In this work, we consider in particular AWE systems with generators installed on the ground which employ curved kites. In these systems, energy is produced by continuously repeating a two-phase cycle of line extension and retraction. In the first phase, the kite is flown on a path roughly perpendicular to the wind flow (in the so-called crosswind conditions) and develops high pulling forces, hence generating power during line reel-out. In the second phase, the kite is maneuvered in such a way that its lift is reduced, and a fraction of the previously generated energy is spent to reel-in the lines. Examples of companies developing such systems include Skysails GmbH [3], Kitenergy [4], and EnerKite [5]. Like most airborne wind energy systems, ground-based AWE generators rely heavily on automatic control during operation. The control tasks are essentially two: stabilize the wing's flight pattern, typically a figure-eight shape during power generation, and control the line reeling in order to maximize the average power. The variables that can be manipulated to achieve these tasks are the so-called steering deviation, which can be obtained by means of either onboard actuators or ground based ones (for multi-lined kites), and the line force, which is set by controlling the torque of the generator on the ground. In recent years, several studies have appeared, concerned with the modeling and control of flexible wings to achieve figure-eight patterns, see e.g. [6], [7], [8], showing that this control task can be achieved with relatively simple and quite robust approaches, using only the steering deviation as input variable and hence leaving the line

force as free variable to control the line reeling. Indeed the mentioned steering controllers have been also used together with quite standard strategies that manipulate the line force to achieve the mentioned power production cycles, see e.g. [1] (Part IV) and [9]. In addition to the steering deviation and the line force, many AWE system also feature a third control variable, i.e. the pitch angle of the wing, which in principle can be used to improve the system's performance. A change of the pitch angle produces directly a change of the angle of attack of the wing, which in turn influences the aerodynamic lift and drag coefficients, hence changing the aerodynamic forces and the flight speed. For rigid wings, like those used by Ampyx power [1] (Ch. 26) and Makani power [10], the dependency of the lift and drag forces on the angle of attack is well-studied, and established techniques and actuators can be used to control this variable, which can be estimated with good accuracy. On the other hand, when flexible curved kites are used the situation is much different: in this case the aerodynamics have been much less investigated in the literature and the angle of attack is harder to estimate, hence making the explicit use of this variable for feedback control not viable. Indeed there are few studies that consider the use of active pitch control in kites for airborne wind energy. In [11], optimal power cycles for power generating kites have been studied, considering also the derivative of the lift coefficient among the available inputs. However, it is not explicitly mentioned how the lift coefficient derivative can be manipulated in practice with the required accuracy. The dependency of the lift and drag coefficients on the angle of attack for a curved wing has been studied in [12] and the results have been used e.g. in [13] to study kite-based AWE systems but without considering the use of an active pitch strategy.

In this paper, we provide two main contributions towards the effective use of active pitch control in AWE systems that employ curved kites. The first contribution is a new computational fluid dynamics (CFD) study of the aerodynamics of such wings, where we account for the three-dimensional effects. The approach we use for this study has been also validated with experimental data [14], hence increasing the confidence in the results. Building on the findings of the aerodynamic analysis, as a second contribution we propose an active control strategy for the kite pitch, which aims to maximize the average traction force generated during the crosswind patterns. To the best of our knowledge, this is the first time that such an approach is proposed for kite-based airborne wind generators. The proposed controller employs as feedback variable the line force, which is measured with good accuracy, hence avoiding the need to estimate the angle of attack and the problems related to the estimation

The authors are with the ABB Switzerland Ltd., Corporate Research, 5405 Baden-Dättwil - Switzerland

* E-mail addresses: { marcelo.buffoni | bernardo.galletti | joachim.ferreau | lorenzo.fagiano | mehmet.mercangoez }@ch.abb.com

errors. The manipulated variable is a pitch deviation, which can be issued by adjusting the length of the center line in three-line systems (like the one used in [7] and by [5]) or by suitable onboard actuators in two- and one-line systems. After presenting the aerodynamic study and the active control strategy, we evaluate the effectiveness of the approach through numerical simulations.

II. SYSTEM DESCRIPTION AND MODEL EQUATIONS

A. System layout

We consider a curved flexible wing, or power kite, connected to a ground unit (GU), see Fig. 1 for an example of small-scale prototype with three lines. In three-line systems,



Fig. 1. Example of small-scale prototype built at the University of California, Santa Barbara, employing a curved flexible kite.

the two lateral lines linking the wing to the GU, named steering lines, are attached to the back tips of the wing (see Fig. 1) and they are used to influence its trajectory by applying a steering deviation, δ : a shorter left steering line with respect to the right one impresses a left turn to the wing (i.e. a counter-clockwise turn as seen from the GU), and vice-versa. The center line, named power line, splits into two lines connected to the front of the wing (or leading edge) and sustains about 70% of the generated load. By changing the relative length of the steering lines with respect to the center one, one can change the kite's pitch by an angle denoted by α_0 ("pitch deviation"), which in turn affects the kite's angle of attack, α , and hence the aerodynamic forces. In other systems, like the one-line generator developed at TU Delft (see e.g. [1](Ch. 23)), onboard actuators are used to influence δ and α_0 . On the ground, the lines are rolled around drums, linked to electric generators. Power is produced by making the kite fly fast in crosswind conditions (i.e. roughly perpendicularly to wind flow) and reeling-out the lines (traction phase, see e.g. [13]). When a maximum length of the lines has been reached, some power is spent to reel-in (recovery phase). In this work, we focus on the traction

phase and we employ the control system presented in [7] to manipulate δ in order to achieve consistently figure-eight flight paths. Then, our aim is to address the problem of using α_0 to maximize the produced power. Before introducing our main contributions, we recall the equations of a dynamical model of the considered system, which we need to introduce the main variables of interest and their roles.

B. Model equations

We employ a point-mass model already used in previous works (see e.g. [15] and [7] and references therein), and we recall in particular the equations that model the aerodynamic forces and the angle of attack and link these variables to the control inputs δ and α_0 . We define an inertial frame $G \doteq (X, Y, Z)$, centered at the GU, with the X axis parallel to the ground, contained in the longitudinal symmetry plane of the GU and pointing downwind, the Z axis pointing upwards, and the Y axis to form a right hand system. By denoting the line length with $r(t)$, the wing's position can be expressed in the inertial frame using the spherical coordinates $\theta(t)$, $\phi(t)$, $r(t)$ as:

$${}_G\vec{p}(t) = \begin{pmatrix} r(t) \cos(\phi(t)) \cos(\theta(t)) \\ r(t) \sin(\phi(t)) \cos(\theta(t)) \\ r(t) \sin(\theta(t)) \end{pmatrix}, \quad (1)$$

where t is the continuous time variable. In (1) and throughout the paper, the subscript letter in front of vectors (e.g. ${}_G\vec{p}(t)$) denotes the reference system considered to express the vector components.

We define also a non-inertial coordinate system $L \doteq (L_N, L_E, L_D)$, centered at the wing's position. The L_N axis, or local north, is tangent to the sphere of radius $r(t)$ and points towards its zenith. The L_D axis, called local down, points the center of the sphere (i.e. the GU), hence it is perpendicular to the tangent plane to the sphere at the wing's location. The L_E axis, named local east, forms a right hand system and spans the tangent plane together with L_N . We note that the system L is a function of the wing's position only, and it is different from the local systems used in previous works (see e.g. [13] and the references therein), due to the different definition for angle θ . The kite's motion is influenced by the aerodynamic force, gravity, apparent forces and line traction. In particular, the aerodynamic force $\vec{F}_a(t)$ is given by the contributions of the lift and drag generated by the wing and of the drag induced by the cable. These forces depend on the effective wind speed vector, $\vec{W}_e(t)$, computed as:

$$\vec{W}_e(t) = \vec{W}(t) - \vec{v}(t), \quad (2)$$

where $\vec{W}(t)$ is the wind speed relative to the ground and $\vec{v}(t) \doteq \frac{d}{dt}\vec{p}(t)$ is the wing speed vector. $\vec{F}_a(t)$ can be

computed as (see e.g. [13]):

$$\vec{F}_a(t) = \frac{1}{2}\rho C_L(t)A|\vec{W}_e(t)|^2\vec{z}_w(t) + \quad (3a)$$

$$\frac{1}{2}\rho C_D(t)A|\vec{W}_e(t)|^2\vec{x}_w(t) + \quad (3b)$$

$$\frac{1}{8}\rho C_{D,l}A_l \cos(\Delta\alpha(t))|\vec{W}_e(t)|^2\vec{x}_w(t) \quad (3c)$$

$$= \frac{1}{2}\rho C_L(t)A|\vec{W}_e(t)|^2\vec{z}_w(t) + \frac{1}{2}\rho \underbrace{\left(C_D(t) + \frac{C_{D,l}A_l \cos(\Delta\alpha(t))}{4A} \right)}_{C_{D,eq}(t)} A|\vec{W}_e(t)|^2\vec{x}_w(t). \quad (3d)$$

In (3), the contributions (3a)-(3b) are, respectively, the lift and drag forces generated by the wing, while (3c) is the drag induced by the lines. $C_L(t)$ and $C_D(t)$ are the aerodynamic lift and drag coefficients of the wing, $C_{D,l}$ is the drag coefficient of the lines, A is the reference area of the wing, A_l is the reference area of the lines, ρ is the air density, and $\vec{x}_w(t)$ and $\vec{z}_w(t)$ are the directions of the drag and lift forces, respectively. The parameter $C_{D,eq}(t)$ is called the equivalent aerodynamic drag coefficient, since it accounts for the drag of both the wing and the lines. We note that the aerodynamic coefficients are considered as time-varying parameters here, since they depend on the wing's angle of attack $\alpha(t)$, which in turn changes in time as a function of the flight conditions and of the control input $\alpha_0(t)$. In particular, we have:

$$\alpha(t) = \Delta\alpha(t) + \alpha_0(t), \quad (4)$$

where the variable $\Delta\alpha(t)$ is the angle between the effective wind speed vector $\vec{W}_e(t)$ and the plane spanned by vectors (L_N, L_E) , i.e. the tangent plane to the sphere of radius $r(t)$ at the wing's location. The vectors $\vec{x}_w(t)$ and $\vec{z}_w(t)$, defining the directions of the lift and drag forces (see (3)), depend on the direction of the effective wind and on the roll angle $\psi(t)$ of the wing, which is related to the steering input variable $\delta(t)$. In particular, $\vec{x}_w(t)$ points in the direction of the effective wind $\vec{W}_e(t)$, while $\vec{z}_w(t)$ is perpendicular to $\vec{x}_w(t)$ and to a further vector, denoted by $\vec{e}_t(t)$, which points from the right tip of the wing to the left one, as seen from the GU (see e.g. [13] for a formal definition). Vectors $\vec{x}_w(t)$ and $\vec{z}_w(t)$ can be expressed in the L frame as:

$${}_L\vec{x}_w(t) = \begin{pmatrix} -\cos(\beta(t)) & -\sin(\beta(t)) & 0 \\ -\sin(\beta(t)) & \cos(\beta(t)) & 0 \\ 0 & 0 & -1 \end{pmatrix} \begin{pmatrix} \cos(\Delta\alpha(t)) \\ 0 \\ \sin(\Delta\alpha(t)) \end{pmatrix} \quad (5a)$$

$${}_L\vec{z}_z(t) = \begin{pmatrix} -\cos(\beta(t)) & -\sin(\beta(t)) & 0 \\ -\sin(\beta(t)) & \cos(\beta(t)) & 0 \\ 0 & 0 & -1 \end{pmatrix} \quad (5b)$$

$$\begin{pmatrix} -\cos(\psi(t))\cos(\eta(t))\sin(\Delta\alpha(t)) \\ \cos(\psi(t))\sin(\eta(t))\sin(\Delta\alpha(t)) + \sin(\psi(t))\cos(\Delta\alpha(t)) \\ \cos(\psi(t))\cos(\eta(t))\cos(\Delta\alpha(t)) \end{pmatrix}.$$

In (5), $\psi(t)$ is a function of $\delta(t)$:

$$\psi(t) = \arcsin\left(\frac{\delta(t)}{d_s}\right) \quad (6)$$

where d_s is the wing span; $\eta(t)$ is given by (see e.g. [16]):

$$\eta(t) = \arcsin(\tan(\Delta\alpha(t))\tan(\psi(t))); \quad (7)$$

and $\beta(t)$ is referred to as the heading angle of the wing, and it is computed as the angle between the local north L_N and the effective wind speed $\vec{W}_e(t)$ projected on the (L_N, L_E) plane:

$$\beta(t) = \arctan\left(\frac{\vec{W}_e(t) \cdot \vec{e}_{L_E}(t)}{\vec{W}_e(t) \cdot \vec{e}_{L_N}(t)}\right). \quad (8)$$

In (8), the four-quadrant version of the arc tangent function shall be used, such that $\beta(t) \in [-\pi, \pi]$.

Equations (2)-(8) give an analytic expression for the aerodynamic forces acting on the wing and their links to the control inputs. In the following, we focus on the dependence of the lift and drag coefficients, C_L and C_D , on the angle of attack α and we provide the results coming from a new CFD analysis of a curved kite. Based on these results, we will then propose an approach to manipulate the pitch deviation α_0 in order to maximize the power produced during the traction phase of the energy generation cycle.

III. AERODYNAMIC ANALYSIS OF CURVED WINGS AND ACTIVE PITCH CONTROL STRATEGY

A. 3D CFD analysis of a curved kite

The topic of the evaluation of the aerodynamic forces on a soft kite has been addressed in the literature by means of flow models of different accuracy and complexity. In [13], the aerodynamic data comes from a three-dimensional CFD analysis conducted for a kite with a constant Clark-Y airfoil profile and a circular leading edge extending spanwise of $\pm 45^\circ$ with respect to the kite symmetry plane (see [12]). In [1] (Ch. 16) is shown that the high airfoil camber, typical of soft kites, induces strong flow separation and that such separation exists even for small angles of attack. As a consequence, the authors account for such flow feature in the calculation of their aerodynamic coefficients by using two-dimensional CFD simulations. This approach, however, does not consider the contribution to the aerodynamic forces of the significant three-dimensional effects due to the finite span of the wing and its strong spanwise bending.

In this work the latter issue is addressed by calculating the aerodynamic coefficients through three-dimensional CFD simulations. We derived the geometry of the wing from the small-scale curved flexible kite used in experiments carried out at the University of California at Santa Barbara, see e.g. [17]. Different views of the simplified three-dimensional kite model are shown in Fig. 2. We assumed the kite to be rigid; such an assumption is reasonable during crosswind flight when the kite is subject to quite large loads. The kite's leading edge tube centerline is represented by a semicircle and the wing was symmetric and tapered. In addition, to render the complex meshing procedure somewhat easier, unlike the real kite we considered the airfoil as double membrane. Nonetheless, its leading edge tube, its trailing edge tube and its top boundary were geometrically the same of the actual kite. The kite airfoil cross-section lying on the

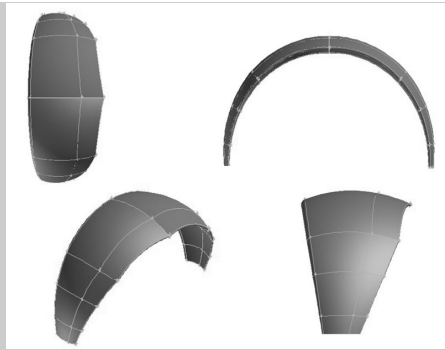


Fig. 2. Top, front, side and isometric view of the kite.

symmetry plane is shown in Fig. 3. It is worth noting that the profile displays the strong camber typical of soft kite wings. The model's main characteristic dimensions are 4.5 meters



Fig. 3. Airfoil considered for the CFD analysis as seen in the kite symmetry plane cross-section.

tip-to-tip distance, 2.64 meters arc height, 1.98 meters root chord and 0.6 meters tip chord.

In terms of root chord units, the computational domain extended for 12 times upstream from the kite, 21 times downstream from it, 13 times above and 12 below, and 14 times in the direction normal to the symmetry plane. Since we assumed symmetric flight conditions for the kite, only one of the symmetric halves of the computational domain was simulated. We divided the computational domain in several mappable sub-volumes, so to have a structured mesh everywhere made of hexahedral elements. The mesh was built in ANSYS GAMBIT 2.4.6 and consisted of 2.5×10^6 cells. We took particular care in dimensioning the boundary layer wrapping the kite in order to have a y^+ value of around 1 for the layer of cells adjacent to the kite surfaces. The boundary layer was made of 17 layers with a first layer thickness of 0.091 mm. The surface mesh on the kite walls consisted of 14,479 rectangular elements, becoming finer towards the wing tip. This was done to better resolve the vortical structures arising in that region which are then transported downstream in the wake. A detail of the surface mesh is shown in Fig. 4.

Once the mesh was completed, we imported it into ANSYS FLUENT 14.0. We set the boundary conditions at the outer surfaces of the computational domain as follows: the front surface as velocity inlet, the back and side surfaces as pressure outlet, the top and bottom surfaces as either velocity inlet or pressure outlet according to whether the far field flow was entering in the domain or exiting from it, respectively.

As for the numerical settings, we used the FLUENT 3D steady pressure-based solver. We employed the simplec method to handle the pressure-velocity coupling, with gradi-

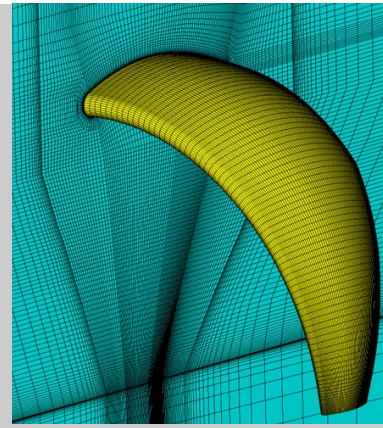


Fig. 4. Detail of the computational grid on kite surfaces and symmetry plane.

ents discretized with the Green-Gauss cell based option. The viscous effects have been represented using the $k-\omega$ SST model. We used a second order upwind spatial discretization scheme for pressure and momentum equations, whereas a first order upwind spatial discretization scheme was used for the turbulent equations. The working fluid was air in either the incompressible or compressible ideal gas approximation depending on the Mach number of the flow at study.

Before carrying out the CFD study on the kite, we validated the mentioned settings by reproducing numerically a wind tunnel experiment of a 45° sweptback wing reported in [14]. In the experiment, the aerodynamic polar was determined for the wing immersed in a flow with a Reynolds number $Re = 4 \times 10^6$ and a Mach number $Ma = 0.2$. For the validation, we carried out four simulations with the air assumed as a compressible ideal gas and for four different angles of attack, i.e. 5° , 10° , 15° and 20° . The differences were measured in terms of the percentile error on the total aerodynamic force coefficient defined as $C_T = \sqrt{C_L^2 + C_D^2}$. Table I summarizes the validation results. It can be seen that the numerical results are in good agreement with the experimental data, giving good confidence in the accuracy of the numerical methodology used for the simulations.

In symmetric flight conditions the only forces and moments at play are lift, drag and pitch moment and for the operative velocities they depend on the angle of attack α , but also on the Reynolds number $Re = V_\infty L / \nu$, i.e. on the upstream far field velocity. We neglected the dependency of the forces on the time derivatives of the angle of attack assuming that the kite is manoeuvred in a way that its flight conditions can be approximated as a sequence of steady states.

We used the numerical setup described above to build an aerodynamic database for characterizing the aerodynamic behavior of the kite model under investigation. In particular, the simulations were run for all possible pairs of angles of attack and upstream velocities in the sets of values $\alpha [^\circ] = 0, 5, 10, 15, 20, 25$ and $V_\infty [m/s] = 1, 2.2, 4.6, 10, 20, 40, 60$. As a consequence, the Reynolds number ranged from 9.9×10^4 to 5.9×10^6 , while the

TABLE I

NUMERICAL VALIDATION OF THE CFD APPROACH: SIMULATED VS. MEASURED AERODYNAMIC COEFFICIENT FOR THE WING [14].

α	$C_{L_{exp}}$	$C_{D_{exp}}$	$C_{T_{exp}}$	$C_{L_{sim}}$	$C_{D_{sim}}$	$C_{T_{sim}}$	% $C_{T_{err}}$
5°	0.322	0.011	0.322	0.325	0.018	0.325	0.9
10°	0.590	0.027	0.591	0.618	0.035	0.619	4.5
15°	0.819	0.082	0.823	0.788	0.086	0.793	3.8
20°	1.000	0.198	1.019	0.911	0.241	0.942	8.4

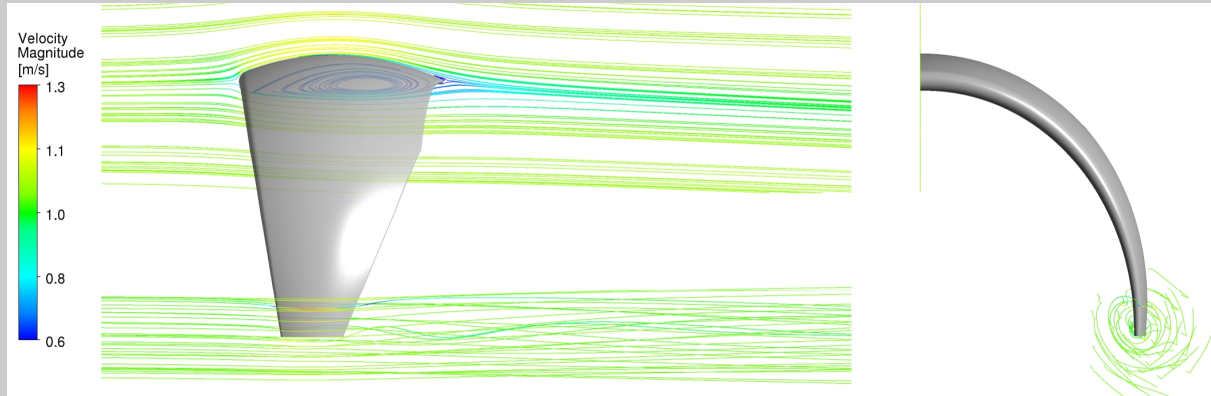


Fig. 5. Flow streamlines around the wind tip and on the symmetry plane for $\alpha = 0^\circ$ and $V_\infty = 1m/s$.

Mach number varied between 0.003 and 0.17. Given these values of the Mach number, the flow was assumed to be incompressible. The validity of this assumption was verified by observing that the difference between the simulation results obtained with the compressible model and those obtained with the incompressible one were negligible for the cases with the largest velocity inlet.

We then computed the coefficients of lift, drag and pitch moment for each simulation in the following way

$$C_L = \frac{L}{1/2\rho V_\infty^2 A}, \quad C_D = \frac{D}{1/2\rho V_\infty^2 A}, \quad C_M = \frac{M}{1/2\rho V_\infty^2 AL}$$

i.e. by dividing the corresponding force by qA and the corresponding moment by qAL , where $q = 1/2\rho V_\infty^2$ is the dynamic pressure at the upstream boundary of the domain. In these relationships ρ , L , A , and V_∞ are density, characteristic length, characteristic area and velocity respectively. In particular, A was set equal to one half of the kite mean surface ($A = 6.06 m^2$) since only one of the two symmetric halves of the flow domain is solved for, whereas L was assumed equal to the mean aerodynamic chord

$$L = \frac{1}{A} \int_{halfspan} c^2(s) ds,$$

where s is the curvilinear coordinate along the leading edge centerline and c is the local kite chord. The air density was set equal to $1.225 kg/m^3$. The values for ρ , L , A are provided as reference values and do not vary throughout the simulations.

Each simulation was deemed to be converged when the residuals of the equations had dropped by at least four orders of magnitude and the monitored force and moment coefficients became constant. For larger angles of attack

the steady solver exhibited a bad convergence behavior due to a significant vortex shedding from the stalled parts of the kite top surface. In those cases the unsteady solver was used with a suitably small time step. The simulation then were stopped when the monitored force and moment coefficients had reached periodic oscillations. The values taken for the coefficients at convergence were then the mean values averaged over a sufficiently long time interval.

In Fig. 5 the flow streamlines around the wing tip and on the symmetry plane are depicted for $\alpha = 0^\circ$ and $V_\infty = 1 m/s$. The typical tip vortex is clearly shown, as well as a large recirculation zone under the kite bottom surface. The latter is due to the flow separation that takes place at the kite leading edge, even for small angle of attack values, due to the strong camber of the airfoil cross-section.

The simulation results are summarized in Fig. 6 and Fig. 7 in terms of both kite efficiency (i.e. lift to drag ratio) and lift coefficient as a function of the angle of attack for different upstream velocities. It can be seen that for a given value of the inlet velocity the efficiency curves have a maximum at approximately 10° . Moreover the maximum value for the $C_L(\alpha)$ curves occurs at about 15° , that is for values of α larger than those that maximize the efficiency.

The described CFD analysis provided us with a new set of lift and drag coefficients as a function of the wing's angle of attack. The main added value of the coefficients computed in this work with respect to those used previously in the literature (see e.g. [13]) is that the considered geometry is much closer to that of a curved power kite, that the employed computational method takes into account 3D effects neglected by previous analyses, and that the approach has been previously validated against experimental data. In the next section, we exploit the outcome of the CFD analysis

to address the problem of controlling the pitch deviation α_0 in order to increase the power generated during the traction phase of the energy generation cycle.

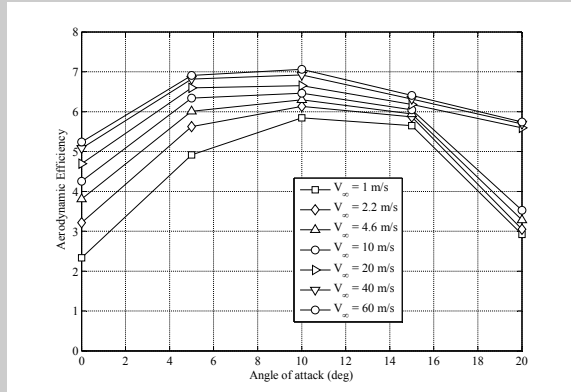


Fig. 6. CFD simulation results. Kite aerodynamic efficiency vs. angle of attack for different upstream velocities.

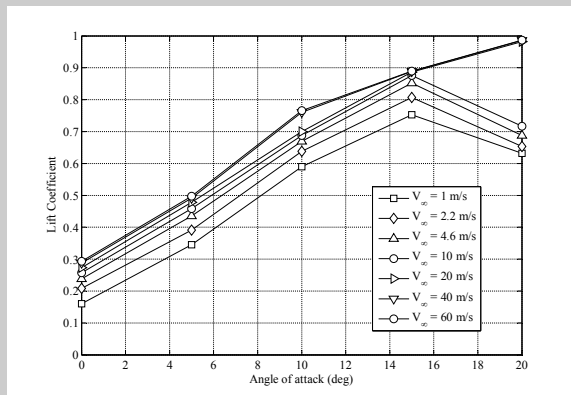


Fig. 7. CFD simulation results. Kite aerodynamic efficiency vs. angle of attack for different upstream velocities.

B. Active pitch control strategy

In order to optimize the power production, one would need to maximize the line force for given flight conditions and tether reel-out speed. To achieve this goal, the kite's angle of attack should be kept within a certain optimal range that depends on the aerodynamics of the kite itself. The idea is to exploit the pitch deviation α_0 to adjust the angle of attack (see e.g. eq. (4)). In order to study this problem, we first carried out a set of closed loop simulations with the model recalled in section II-B, using the aerodynamic coefficients computed with the CFD analysis of section III-A. In the simulations, the kite's steering was controlled by the approach of [7] in order to achieve figure-eight paths. For each simulation, we set a fixed value of the pitch deviation α_0 . The obtained results are shown in Fig. 8, where the traction force (averaged over one figure-eight cycle) is plotted as a function of α_0 . For a given reel-out speed, the power produced is directly proportional to

the average traction force. From the plot of Fig. 8, two important observations can be made: first, operating the kite with a suboptimal choice of α_0 may reduce power production significantly. Second, the 3D CFD model as proposed in section III suggests that the generated force as function of α_0 is quasi-concave, hence one can in principle compute the value of the angle of attack which maximizes the line force, and then design a controller that manipulates the the pitch deviation α_0 to track such an optimal angle of attack.

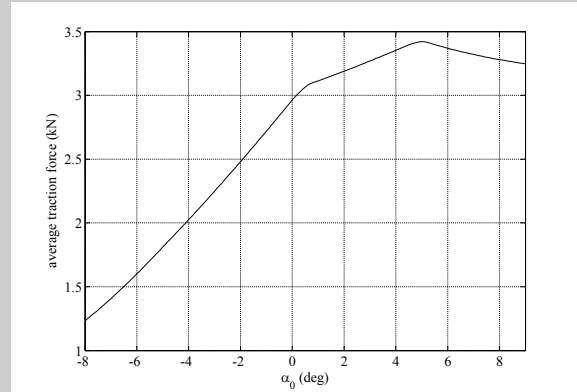


Fig. 8. Simulation analysis. Average traction force vs. control input α_0 according to proposed CFD model.

However, an attempt to control the angle of attack directly would give rise to at least three significant issues. The first one is that, differently from standard rigid wings, the angle of attack is very difficult to estimate or measure for curved kites, like the ones used in the existing prototypes of airborne wind energy generators, hence making this variable not suited for feedback control. The second problem is that the effect that the pitch deviation has on the angle of attack (see eq. (4)) is not known exactly, rather it is prone to uncertainties. In this respect, a reasonable assumption is that by increasing or decreasing the pitch deviation one is able to increase or decrease the angle of attack, but it is unrealistic to assume that the latter can be set to a specific numerical value. In fact, it is possible to set the pitch actuator to a desired position, but the actual change of pitch angle (hence of angle of attack) corresponding to such a position is uncertain. Finally, a third issue is given by the fact that the computed aerodynamic coefficients are still subject to uncertainty, so that one can not rely solely on those curves to compute a reference, optimal angle of attack.

In order to overcome all these problems, we propose here to use a simple feedback control strategy to maximize the traction force during operation of the kite. As the pitch angle and the angle of attack are difficult to be measured or controlled in case of flexible kites, we propose to adjust α_0 using directly the traction force on the line as feedback variable. The latter is indeed easy to measure with good accuracy. In particular, since we are interested in the average force, we use as feedback variable the mean force over a fixed number of $n \geq 1$ figure-eight cycles. In this way, the effects of wind turbulence are also mitigated. The start of a

new cycle can be detected easily and reliably by observing the crossings of the azimuthal angle $\phi(t)$ at its mean value. This yields a one-dimensional function

$$F_n : \mathbb{R} \rightarrow \mathbb{R}$$

$$\alpha_0 \mapsto F_n(\alpha_0).$$

The actual adjustment of α_0 to find a value that maximizes $F_n(\alpha_0)$ can be done in different ways. As evaluating derivatives of this function through finite-differences might prove cumbersome due to measurement noise, we suggest to employ a simple search algorithm for optimizing F_n with respect to α_0 as summarized in Algorithm 1.

Algorithm 1 Pitch Adaptation

Input: $\alpha_0(t_i), \Delta\alpha_0(t_i), F_n(\alpha_0(t_i)), F_n(\alpha_0(t_{i-1}))$

Output: $\alpha_0(t_{i+1}), \Delta\alpha_0(t_{i+1})$

```

if  $|\Delta\alpha_0(t_i)| > \Delta_{\min}$  then
  if  $F_n(\alpha_0(t_i)) \geq F_n(\alpha_0(t_{i-1}))$  then
     $\Delta\alpha_0(t_{i+1}) \leftarrow -\frac{1}{2}\Delta\alpha_0(t_i)$ 
  else
     $\Delta\alpha_0(t_{i+1}) \leftarrow \Delta\alpha_0(t_i)$ 
  end if
   $\alpha_0(t_{i+1}) \leftarrow \alpha_0(t_i) + \Delta\alpha_0(t_{i+1})$ 
else
   $\alpha_0(t_{i+1}) \leftarrow \alpha_0(t_i)$ 
   $\Delta\alpha_0(t_{i+1}) \leftarrow \Delta\alpha_0(t_i)$ 
end if

```

This procedure can be started at any time t_i (corresponding to the i th start of a sequence of n figure-eight cycles) by making an initial change $\Delta\alpha_0(t_i) > \Delta_{\min}$ to the current control input $\alpha_0(t_i)$. As the step size $\Delta\alpha_0$ is never increased and decreased by a constant factor whenever the last step reduced the average traction force F_n , this procedure is guaranteed to converge to a constant value of α_0 after a finite number of cycles. Moreover, it is easy to see that it will always find the optimal value of α_0 if F_n is a quasi-concave function. Note that this simple pitch control strategy does not require any model of the actuator's or system's dynamics nor knowledge of the aerodynamic coefficients: the only underlying assumption is that the *qualitative* behavior of the traction force as a function of the pitch angle is like the one predicted by the CFD analysis of section III. Finally, it can be noted that, by acting through an incremental change $\Delta\alpha_0$ of the pitch deviation, the approach is able to reject eventual constant disturbances acting on the pitch deviation itself, e.g. due to a tracking error in the low level controller for the pitch actuator.

IV. SIMULATION RESULTS

We will now present simulation results based on the kite model described in section II using the aerodynamic coefficients obtained by the CFD analysis of section III-A and applying the pitch controller of section III-B. In the simulation, we use a logarithmic wind shear model with wind speed of 5 m/s at 32.5 m of altitude, and parameter

$6 \cdot 10^{-4}$ m (see e.g. [13]). We set an initial value of $\alpha_0(t_0) = -0.9$ (deg). We average the traction force over $n = 1$ full figure-eight cycles and start with an initial change of $\Delta\alpha_0 = 1$ deg after 25 seconds.

Fig. 9 shows how the pitch adaptation algorithm adjusts the control input α_0 and steers it to its optimal value. We recall that this optimal value is only known in simulations and that the adaptation procedure does not require any knowledge about it to run successfully. The corresponding average traction force is shown in Fig. 10, again comparing it to its theoretical optimal value.

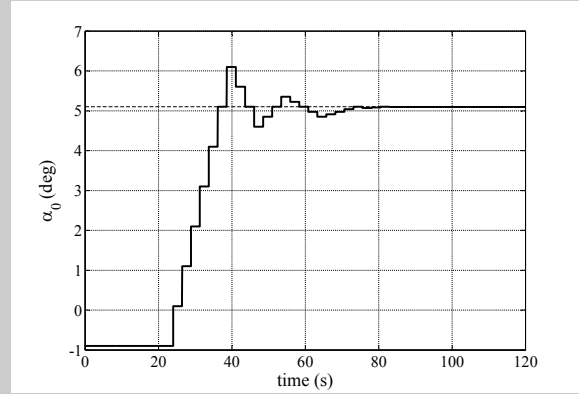


Fig. 9. $\alpha_0(t)$ is automatically adapted during the simulation (solid line); also the optimal value is shown (red, dotted).

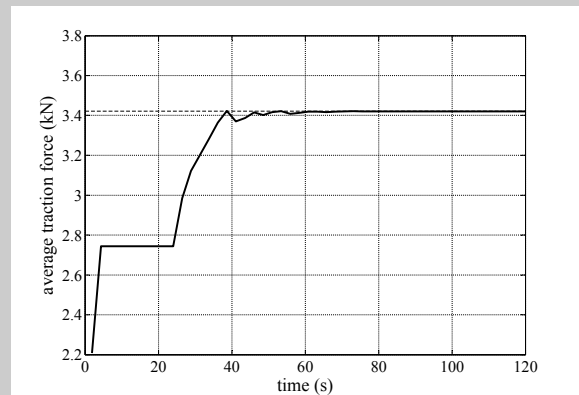


Fig. 10. Average traction force F_1 during the simulation (solid line); also the optimal value is shown (red, dotted).

Fig. 11 depicts the angle of attack $\alpha(t)$ as resulting from the adjustments of α_0 . Fig. 12 and Fig. 13 illustrate the corresponding continuous traction force and kite trajectory in spherical coordinates, respectively. In our case, optimizing the angle of attack slightly reduces the aerodynamic efficiency, but increases $C_L(t)$ even more; as a consequence, the steering gain of the kite increases (see [7] for more details), leading to slightly tighter kite trajectories.

Finally, we note that further simulations have confirmed that the proposed controller also works well in the presence of turbulent wind conditions.

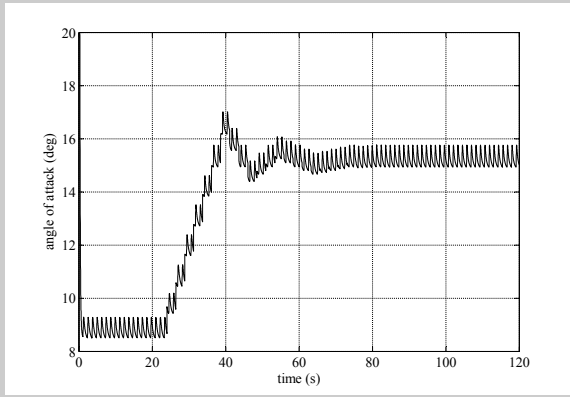


Fig. 11. Angle of attack $\alpha(t)$ as automatically adapted during the simulation.

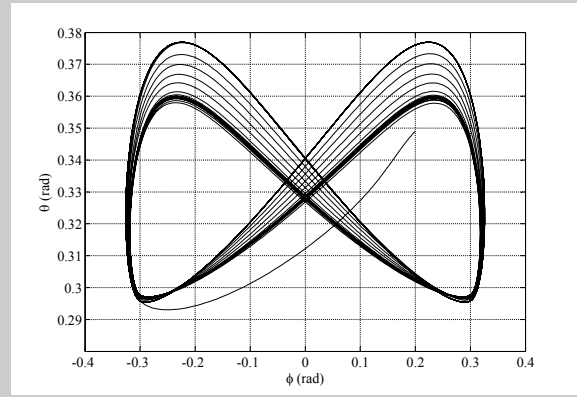


Fig. 13. Kite trajectory in spherical coordinates during the simulation.

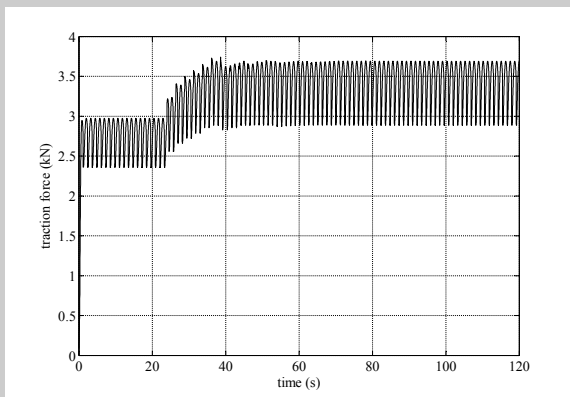


Fig. 12. Traction force during the simulation.

V. CONCLUSIONS

We presented a study on the use of active pitch control to maximize the power produced by an airborne wind energy system that uses a curved kite. The approach exploits the outcome of a new CFD analysis of a curved kite, using a method that has been benchmarked against experimental results. The advantages of the proposed technique is that it employs only the measured traction force, without the need to estimate the kite's angle of attack. Moreover, the only underlying assumption is that the qualitative shape of the traction force as a function of the wing's angle of attack is like the one predicted by our CFD study, while the exact quantitative values are irrelevant for the sake of convergence to the maximum. We showed the effectiveness of the approach through numerical simulations.

ACKNOWLEDGMENTS

The authors thank Ms Laree Block (University of Calgary) for performing some of the CFD simulations.

REFERENCES

[1] U. Ahrens, M. Diehl, and R. Schmehl, Eds., *Airborne Wind Energy*, ser. Green Energy and Technology. Springer-Verlag Berlin, 2013.

- [2] L. Fagiano and M. Milanese, "Airborne wind energy: an overview," in *American Control Conference 2012*, Montreal, Canada, 2012, pp. 3132–3143.
- [3] SkySails GmbH & Co., 2010, <http://www.skysails.info>.
- [4] Kitenenergy website, <http://www.kitenenergy.net/>.
- [5] Enerjite GmbH website, <http://www.enerkite.com/>.
- [6] M. Erhard and H. Strauch, "Control of towing kites for seagoing vessels," *IEEE Transactions on Control Systems Technology*, vol. 21, no. 5, pp. 1629 – 1640, 2013.
- [7] L. Fagiano, A. Zraggen, M. Morari, and M. Khammash, "Automatic crosswind flight of tethered wings for airborne wind energy: modeling, control design and experimental results," *IEEE Transactions on Control Systems Technology*, 2013, doi: 10.1109/TCST.2013.2279592. In press, online version available.
- [8] L. Fagiano, K. Huynh, B. Bamieh, and M. Khammash, "On sensor fusion for airborne wind energy systems," *IEEE Transactions on Control Systems Technology*, 2012, doi:10.1109/TCST.2013.2269865. In press, online version available.
- [9] A. Zraggen, L. Fagiano, and M. Morari, "Automatic retraction phase of airborne wind energy systems," in *19th IFAC World Congress (to appear)*, Cape Town, South Africa, 24-29 August 2014, 2014.
- [10] Makani Power Inc., <http://www.makanipower.com>.
- [11] A. Ilzhöfer, B. Houska, and M. Diehl, "Nonlinear MPC of kites under varying wind conditions for a new class of large-scale wind power generators," *International Journal of Robust and Nonlinear Control*, vol. 17, pp. 1590–1599, 2007.
- [12] G. M. Maneia, "Aerodynamic study of airfoils and wings for power kites applications," Master's thesis, Politecnico di Torino, October 2007, <http://lorenzofagiano.altervista.org/MasterThesisManeia.pdf>.
- [13] M. Canale, L. Fagiano, and M. Milanese, "High altitude wind energy generation using controlled power kites," *IEEE Transactions on Control Systems Technology*, vol. 18, no. 2, pp. 279 –293, mar. 2010.
- [14] W. Schneider, "A comparison of the spanwise loading calculated by various methods with experimental loadings obtained on a 45 degree sweptback wing of aspect ratio 8.02 at a reynolds number of 4.0×10^6 ," NACA, Tech. Rep., January 1954, technical Report 1208.
- [15] M. Diehl, "Real-time optimization for large scale nonlinear processes," Ph.D. dissertation, University of Heidelberg, Germany, 2001.
- [16] I. Argatov, P. Rautakorpi, and R. Silvennoinen, "Estimation of the mechanical energy output of the kite wind generator," *Renewable Energy*, vol. 34, p. 1525, 2009.
- [17] L. Fagiano and T. Marks, "Design of a small-scale prototype for research in airborne wind energy," *arXiv 1307.4215*, 2013.